

# ac-mode atomic force microscope imaging in air and solutions with a thermally driven bimetallic cantilever probe

Andrew C. Hillier<sup>a)</sup> and Allen J. Bard

*Department of Chemistry and Biochemistry, University of Texas at Austin, Austin, Texas 78712*

(Received 5 August 1996; accepted for publication 10 February 1997)

An ac imaging mode for atomic force microscopy (AFM) has been developed that employs a thermally driven bimetallic cantilever to sense surface topography. Oscillations are induced in a composite cantilever, comprising a  $\text{Si}_3\text{N}_4$  layer and Au overcoat, by local heating with a resistive wire heater placed in close proximity to the cantilever. Cantilever bending occurs upon heating due to the difference in thermal expansion coefficients of the  $\text{Si}_3\text{N}_4$  and Au layers. The magnitude of this bending is a function of the heat input, the cantilever geometry, the frequency of the excitation, and the thermal properties of the surrounding medium. A commercially available contact mode AFM has been modified to perform ac mode imaging by driving the cantilever with a peak-to-peak amplitude of 5–15 nm using resistive heating. The heating frequency was typically fixed near the cantilever's resonance frequency, which was in the range of 15–50 kHz in the air and 2–15 kHz in solution for the cantilevers used here. Simultaneous cantilever deflection and amplitude measurements during sample approach indicate that the cantilever free amplitude is damped upon surface contact. While imaging, a fixed damping of the cantilever oscillation is used as a feedback signal to maintain a constant tip-sample separation. Images with this ac imaging mode were obtained in both air and liquid environments. Results show an improvement in image quality in the ac mode over the corresponding contact images, which is the result of a decrease in lateral forces with an oscillating tip. This provides a simple and robust method for ac-mode AFM imaging in air and solutions that can be achieved with only slight modification to a commercially available contact-mode microscope. © 1997 American Institute of Physics. [S0034-6748(97)04605-4]

## I. INTRODUCTION

The atomic force microscope (AFM) is a versatile tool for surface imaging that can be used in ambient, vacuum, and liquid environments.<sup>1</sup> In the typical imaging mode, a flexible cantilever with a sharp tip is placed in close proximity to a sample surface. Tip position is monitored with optical<sup>2</sup> or capacitive methods,<sup>3</sup> and surface images are acquired by physically dragging this tip across the surface of interest. Generally, a feedback mechanism is employed such that a system parameter, typically the cantilever deflection and thus the applied force, is maintained at a constant value by varying the sample position and mapping the surface topography via the applied piezo voltages. The resulting images reflect nominally constant force conditions. A major limitation of this "contact mode" of imaging, where the tip is in physical contact with the sample surface, results from the presence of lateral tip-sample forces.<sup>4</sup> These lateral forces serve to increase sample degradation, which can be considerable for soft materials, and to obscure surface features, which reduces microscope resolution.

These limitations can be overcome by employing non-contact or ac operating modes. In ac-mode imaging, the cantilever is forced to oscillate via some external excitation, which can be derived from piezoelectric,<sup>5</sup> magnetic,<sup>6</sup> photo-thermal,<sup>7</sup> or acoustic sources.<sup>8</sup> When driven at a constant input excitation, free cantilever oscillations will be damped as the tip approaches a surface through an interac-

tion with near-field forces, much in the way a static cantilever bends in response to these forces. Several ac-mode microscopes based upon an oscillating cantilever tip, which involve either noncontact or intermittent contact between the tip and sample while imaging, have been developed for use in air and vacuum.<sup>5,7</sup> However, development of similar techniques that operate in liquid environments, where the reduced forces associated with noncontact imaging are most beneficial, has been somewhat limited. Methods that have proved successful in producing sufficient tip oscillation for imaging in solutions include magnetically,<sup>6,9</sup> piezoelectrically,<sup>10</sup> and acoustically<sup>8</sup> driven cantilevers.

In the work reported here, an ac mode of AFM imaging is described that employs a standard contact mode microscope in which a resistive heater is used to excite cantilever oscillations. Cantilever bending is achieved by a bimetallic effect that is induced via the inequivalent expansion of gold and  $\text{Si}_3\text{N}_4$  layers in a composite cantilever probe as a function of the temperature of the surrounding media. During image acquisition, the cantilever is driven at resonance by temperature fluctuations produced at a resistive heater. The excitation frequency of the heater is set to the cantilever's resonance frequency. Images are acquired by extracting the amplitude of tip oscillation as a function of sample position and using that as a feedback parameter to drive microscope operation. Imaging is achieved in both ambient and solution environments. Results indicate an improvement in image quality in the ac mode over the corresponding contact images. This provides a simple and robust method for ac-mode AFM imaging in air and solutions that can be achieved with

<sup>a)</sup>Current address: Department of Chemical Engineering, University of Virginia, Charlottesville, VA 22902.

only slight modification to commercially available contact-mode microscopes.

## II. EXPERIMENT

### A. Materials

A variety of substrates were used for imaging, including graphite, freshly cleaved mica, and a polished NiCr/Delrin assembly. The Ni-Cr wire/Delrin assembly was sealed with epoxy (Torr Seal, Varian) and polished to optical smoothness with successively finer grades of silica slurry (Buehler, Lake Bluff, IL) so that a smooth Ni-Cr segment was left exposed in the Delrin support. The wire had an exposed area of  $7.06 \times 10^{-4} \text{ cm}^2$  and served as both a substrate for imaging and also as a source for resistive heating, which was accomplished by passing a current through the wire. The Ni-Cr wire had a resistivity of  $100 \times 10^{-6} \Omega \text{ cm}$  and an exposed area with resistance of  $0.0762 \Omega$ , as determined by a four-point resistance measurement. For imaging graphite or mica substrates, a wire heating element was placed near the cantilever.

### B. Atomic force microscope

All experiments were performed with a Nanoscope III atomic force microscope (Digital Instruments, Santa Barbara, CA) equipped with probes (Nanoprobe, Park Scientific, Sunnyvale, CA) consisting of triangular  $\text{Si}_3\text{N}_4$  cantilevers with integrated pyramidal tips. A piezo scanner having a maximum scan range of  $15 \mu\text{m} \times 15 \mu\text{m} \times 2 \mu\text{m}$  was used for sample positioning. The cantilevers had a nominal  $\text{Si}_3\text{N}_4$  thickness of 600 nm, with an additional reflective Au coating of approximately 40 nm and a Cr undercoat of 5–10 nm. Several cantilever sizes, with different spring constants and resonant frequencies, were used. These included cantilevers with manufacturer's reported spring constants of 0.56, 0.32, 0.12, and  $0.06 \text{ N m}^{-1}$  and resonant frequencies ranging from 47 to 17 kHz in air. In purified  $\text{H}_2\text{O}$ , these resonance frequencies decreased to approximately 12 and 3 kHz for the 100- and 200- $\mu\text{m}$ -long cantilevers, respectively.

Solution measurements were carried out in a fluid cell (Digital Instruments, Santa Barbara, CA) with Teflon tubing [Fig. 1(a)]. All fluid cell components were cleaned immediately before use by an extensive soak in purified water and rinsed in EtOH, rinsed with copious amounts of purified water, and dried under nitrogen. The substrate was mounted to the three-dimensional tube scanner via a magnetic sample disk. Electrical connection to the heating element was made through the back of the sample disk.

### C. ac measurements

A schematic of the thermally driven noncontact AFM appears in Fig. 1(a). Detection of cantilever oscillation was achieved by extracting the deflection signal  $(A-B)/(A+B)$  from the sectored photodiode detector following the preamplifier. This signal was then fed into a lock-in amplifier (Model 5201, EG&G, Princeton, NJ) with a reference signal provided by a function generator (Model 2400 AM/FM/phase lock generator, Krohn-Hite Corp., Avon, MA). The

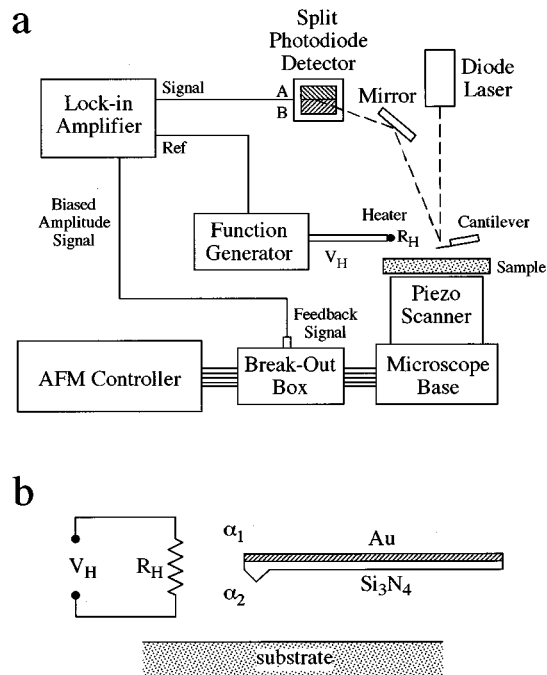


FIG. 1. (a) Schematic diagram of thermally driven ac-mode AFM with related electronics. The cantilever is excited thermally by a heating voltage of  $V_H$  through a resistor  $R_H$ . (b) Schematic of thermally driven bimetallic cantilever probe. The cantilever comprises a bimetallic beam of  $\text{Si}_3\text{N}_4$  and Au with thermal expansion coefficients of  $\alpha_{\text{Si}_3\text{N}_4} = 3.2 \times 10^{-6} \text{ K}^{-1}$  and  $\alpha_{\text{Au}} = 14.2 \times 10^{-6} \text{ K}^{-1}$ , respectively.

function generator also served as the power supply for resistive heating. A sine or square wave excitation was used for heating with a peak-to-peak heating voltage of  $V_H$  and a heating frequency of  $f_H$ . The heating power  $I^2R$  was determined by measuring the current through a standard resistor.

A lock-in amplifier served to rectify and filter the oscillatory component of the deflection signal, giving a peak-to-peak amplitude. Alternatively, the deflection signal could be passed through a circuit comprising, in order, a full-wave rectifier, low-pass filter, and voltage amplifier. This would convert the ac deflection signal to a peak-to-peak amplitude in a fashion similar to that of the lock-in. In the arrangement depicted in Fig. 1(a), the amplitude signal of the lock-in amplifier was fed back into the AFM via a home-built break-out box, which was placed between the microscope controller and base and allowed access to the feedback signal, microscope bias, piezovoltages, and several auxiliary channels. Cantilever oscillations in normal contact mode imaging were monitored by feeding the amplitude signal into the microscope through an auxiliary channel. For ac-mode imaging, the deflection feedback signal was replaced with the amplitude signal from the lock-in. The amplitude signal was biased with a set point voltage, corresponding to a fixed amplitude damping, by subtracting a fixed voltage from the amplitude signal with a simple adder circuit. For imaging, the heating frequency was typically fixed near the cantilever resonance frequency, which was in the range of 15–50 kHz in air and 2–15 kHz in  $\text{H}_2\text{O}$  for the cantilevers used here. This limited acquisition time for imaging to approximately 1 Hz and below. For a  $256 \times 256$  pixel image, this required

approximately 20 min per image. Faster imaging was limited to the resonance cycle of the cantilever and could be improved by using tips with higher resonance frequencies. The separation between heater and cantilever proved a minor factor in the cantilever response, because the entire cell volume was heated with the resistor and the distance between heater and cantilever simply introduced a phase lag in the response with minimal damping of the cantilever oscillations.

### III. THERMAL RESPONSE OF BIMETALLIC CANTILEVER

A difference in thermal expansion coefficients  $\alpha$  between the layers in a bimetallic beam leads to a bending effect in response to changes in temperature. Theories concerning the mechanical response of a bimetallic beam are well-developed and can be found in several standard texts.<sup>11</sup> The cantilever in an AFM is simply a bimetallic beam of small dimensions in which the bending effect can be measured to high sensitivity with the standard AFM tip-sensing mechanism. The temperature sensitivity of an AFM cantilever has been exploited to develop a femtojoule calorimeter,<sup>12</sup> to examine the heat generated during a gas-phase catalytic reaction,<sup>13</sup> and for thermal imaging.<sup>14</sup>

When placed in a constant temperature bath, the cantilever acts as a highly sensitive thermometer. A change in the bath temperature results in a cantilever deflection governed by

$$d = 3(\alpha_2 - \alpha_1)$$

$$\times \frac{t_1 + t_2}{t_2^2 \left[ 4 + 6 \left( \frac{t_1}{t_2} \right) + 4 \left( \frac{t_1}{t_2} \right)^2 + \frac{E_1}{E_2} \left( \frac{t_1}{t_2} \right)^3 + \frac{E_2}{E_1} \left( \frac{t_2}{t_1} \right) \right]} \Delta T l^2 \quad (1)$$

where  $d$  is the deflection at the free end of the cantilever ( $x=0$ ),  $l$  is the cantilever length,  $\Delta T$  is the temperature change as a function of  $x$ ,  $\alpha_i$  is the thermal expansion coefficient ( $\alpha_{\text{Si}_3\text{N}_4} = 3.2 \times 10^{-6} \text{ K}^{-1}$ ,  $\alpha_{\text{Au}} = 14.2 \times 10^{-6} \text{ K}^{-1}$ ),  $E_i$  is Young's modulus ( $E_{\text{Si}_3\text{N}_4} = 1.8 \times 10^{11} \text{ N m}^{-2}$ ,  $E_{\text{Au}} = 0.8 \times 10^{11} \text{ N m}^{-2}$ ), and  $t_i$  represents the thickness of layers 1 and 2. Thus, the tip deflection is proportional to the temperature change  $\Delta T$  and the square of the cantilever length  $l$ .

In the experiments performed here, the cantilever had a triangular shape with two legs, which approximated the response of a rectangular beam.<sup>15</sup> The cantilever comprised a  $\text{Si}_3\text{N}_4$  layer of 600 nm thickness and a Au overcoat of approximately 40 nm thickness [Fig. 1(b)]. A thin Cr anchor (5–10 nm) is placed between the Au and  $\text{Si}_3\text{N}_4$  layers to improve adhesion. In these experiments, the cantilever was housed in the AFM fluid cell, which had a fixed volume defined by the enclosure between the upper quartz surface, the lower substrate, and the sidewalls being an o-ring. Because the thermal expansion coefficient of the Au layer is higher than that of the  $\text{Si}_3\text{N}_4$  layer, an increase in temperature near the cantilever produced a downward bend at the free end of the cantilever. Temperature changes were produced by resistive heating of a small Ni-Cr wire located in the vicinity of the cantilever. According to Eq. (1), the tem-

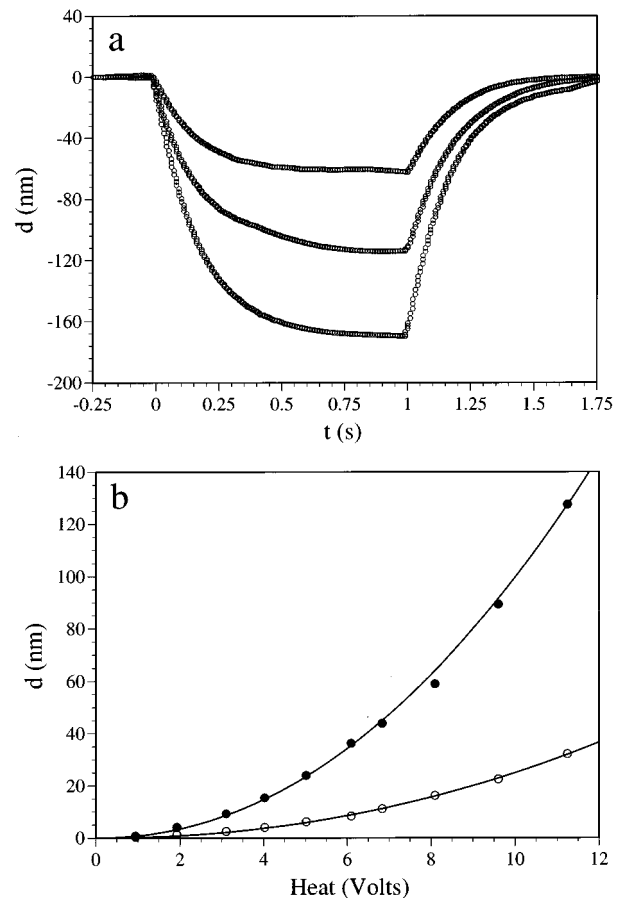


FIG. 2. Deflection of bimetallic cantilever in response to constant heat input. (a) Deflection vs time for heat steps of  $V_H = 7, 10,$  and  $13 \text{ V}$  (0.64, 1.31, and 2.22 mW). (b) Deflection vs heating voltage for 200- $\mu\text{m}$  (filled circles) and 100- $\mu\text{m}$ -long (empty circles) cantilevers. The solid lines represent a best linear fit of cantilever deflection versus power (power= $I^2R$ ). The best fit cantilever response is  $d \text{ (nm)} = 90 \pm 5$  and  $22 \pm 4 I^2R \text{ (mW)}$  for the 200- $\mu\text{m}$  and 100- $\mu\text{m}$  cantilevers, respectively.

perature sensitivities of the 200  $\mu\text{m}$  and 100  $\mu\text{m}$  cantilevers used here were 97.2 and 24.3  $\text{nm K}^{-1}$ , respectively.

When a constant voltage was applied to the resistive heater in air, the temperature near the cantilever increased and the response shown in Fig. 2(a) was obtained. In these experiments, a 1-s potential step to several different heating values  $V_H$  was applied at  $t=0$ . The tip responded by quickly bending downward with a characteristic decay length before approaching a steady-state deflection that was a function of the heating voltage. The deflection was greater for larger values of  $V_H$ . After removing the heating voltage, the temperature near the cantilever decreased and the cantilever responded by bending back to its initial geometry. The heating and cooling cycles exhibited a similar time constant.

The steady-state cantilever deflection increased with increasing applied heating voltage [Fig. 2(b)]. For the resistor value used here ( $R_H = 0.0762 \text{ }\Omega$ ), the response to heating voltages between 0 and 12 V ranged from 0 to 130 nm for the 200- $\mu\text{m}$  cantilever and 0 to 30 nm for the 100- $\mu\text{m}$  cantilever. The increase in steady-state deflection in both fits a characteristic parabolic increase with heating voltage, which indicates that the cantilever deflection is linear with the heating power  $I^2/R$ . A fit of tip deflection to heating power

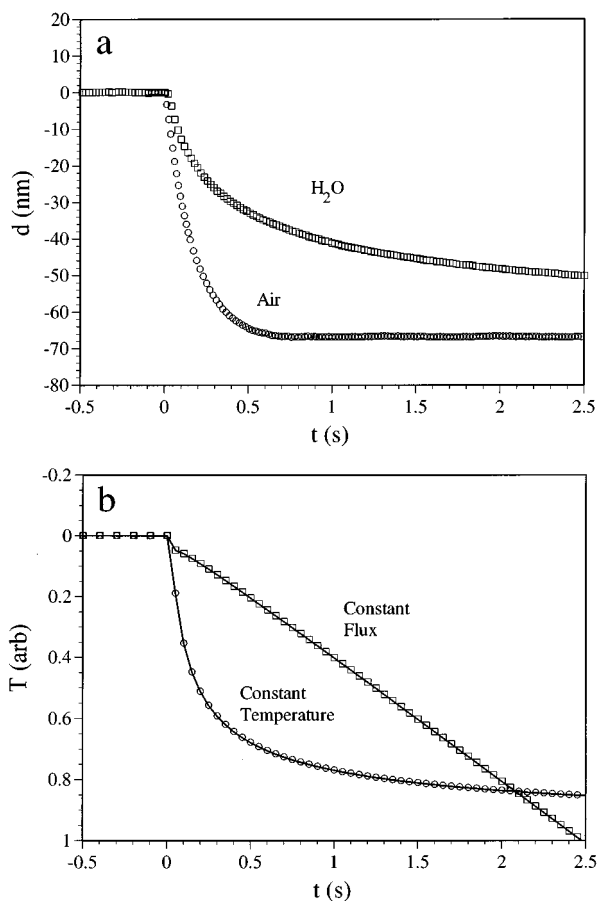


FIG. 3. (a) Deflection of bimetallic cantilever in response to constant heat input of 0.84 mW in air (empty circles) and H<sub>2</sub>O (empty squares). (b) Theoretical temperature response given by Eqs. (2) and (3) for semi-infinite solid with wall at constant temperature (empty circles) and constant heat flux (empty squares).

[solid lines in Fig. 2(b)] provides a sensitivity of  $90 \pm 5$  and  $22 \pm 4$  nm mW<sup>-1</sup> for the 200- $\mu\text{m}$  and 100- $\mu\text{m}$  cantilevers, respectively. According to Eq. (1), the cantilever deflection is proportional to the square of the beam length. This response is reflected by the observed sensitivities to heating power, where the ratio of sensitivities is 4.1:1 and the ratio of lengths is 2:1.

The cantilever responded to resistive heating by a downward deflection in both gas phase and solution environments. Figure 3(a) depicts the deflection of a 200- $\mu\text{m}$  cantilever in air and purified water following a step to a constant heating value of 0.84 mW. The response in both environments is similar, but with a difference in both the decay length and the steady-state deflection value. Because the AFM fluid cell had a constant volume, a constant heating voltage should produce a continuously increasing cell temperature. However, heat losses in the cell are expected because the quartz cell, substrate, and o-ring are not ideal insulators. Thus, the temperature near the probe increases until a steady-state condition, where the heat input is equal to local heat losses, is reached. This final cell temperature and the rate of temperature increase is a function of the thermal properties of the environment. This behavior can be approximated by treating the cell as a semi-infinite solid and solving Fourier's heat

equation. For a constant temperature step at the surface of a semi-infinite solid, the solution is given by<sup>16</sup>

$$T = T_0 \operatorname{erfc}\left(\frac{x}{2\sqrt{\kappa t}}\right) \quad (2)$$

where  $\operatorname{erfc}$  is the error function complement,  $\kappa$  is the thermal diffusivity, and  $T_0$  is the wall temperature at  $t > 0$ . In the case of a constant temperature flux, which is equivalent to a constant heating rate, the temperature distribution is governed by

$$T = \frac{2F_0\sqrt{\kappa t}}{K} \operatorname{ierfc}\left(\frac{x}{2\sqrt{\kappa t}}\right) \quad (3)$$

where  $F_0$  is the heating rate per unit area given by  $I^2R/A$  and  $K$  is the thermal conductivity. The response predicted by Eq. (3) would be expected only for a perfectly insulating system. The temperature response predicted by Eqs. (2) and (3) at a fixed distance  $x$  from the wall is shown in Fig. 3(b). The behavior corresponding to a constant temperature at the wall [Eq. (2)] more closely resembles that observed by the cantilever deflection, suggesting that the bimetallic cantilever is responding to changes in system temperature, and heat losses through the cell to the surroundings are producing a constant steady-state temperature. The electrical work input to this system by resistive heating  $W_{el}$  can be expressed as

$$-W_{el} = \int_0^t I_H^2 R_H dt \quad (4)$$

where  $I_H$  and  $R_H$  are the heating current and resistance. If the electric heating is done adiabatically and at constant pressure, the work can be related to the enthalpy change  $\Delta H$  and thus the heat capacity  $C_p$  by the relation

$$-W_{el} = \Delta H = C_p(T_0 - T_1). \quad (5)$$

Equations (4) and (5) assume a perfectly insulating environment, which is not a realistic approximation of the AFM cell. However, the system response should reflect the behavior that, for a fixed heat input, a larger heat capacity should be seen with a smaller apparent temperature change, assuming that the heat losses are similar. For the difference observed in air and water [Fig. 3(a)], the larger heat capacity of water ( $C_p = 4.18$  kJ kg<sup>-1</sup> K<sup>-1</sup>) compared to air ( $C_p = 1.87$  kJ kg<sup>-1</sup> K<sup>-1</sup>) is supported by the greater cantilever deflection observed in air. Also, the larger thermal diffusivity of air ( $\kappa = 209$  cm<sup>2</sup> s<sup>-1</sup>) when compared to water ( $\kappa = 1.46$  cm<sup>2</sup> s<sup>-1</sup>) gives a faster temperature response, as governed by Eq. (2).

The experimental data were fit to Eq. (2) to give a time constant  $\tau$  and a steady-state cantilever deflection  $d_{ss}$ , where the cantilever deflection is assumed to correspond to the cell temperature. With the time constant defined by the time required to reach a deflection of 95% of the final value, the tip response gave  $\tau = 2.52$  s in H<sub>2</sub>O and  $\tau = 0.465$  s in air. According to Eq. (2), the ratio of these time constants, which is  $\tau_{\text{H}_2\text{O}}/\tau_{\text{air}} = 5.42$ , should be proportional to the inverse square root of the thermal diffusivities, which is  $(\kappa_{\text{H}_2\text{O}}/\kappa_{\text{air}})^{-1/2} = 11.96$ . The steady-state cantilever deflections in air and water were found to be  $d_{\text{air}} = 67$  nm and

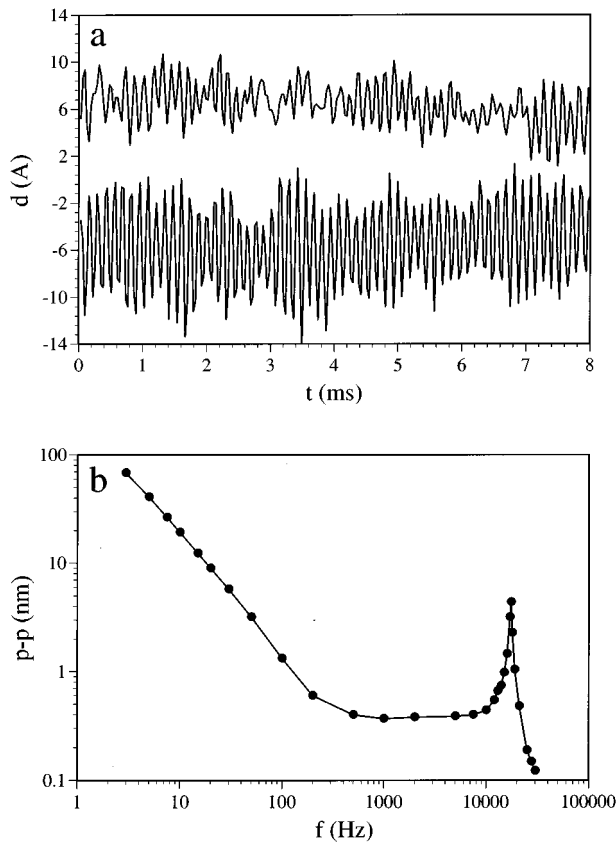


FIG. 4. (a) Time-dependent cantilever oscillations for the 200- $\mu\text{m}$  cantilever in air with no heat input (*upper curve*) and with heat input of 0.47 mW (*lower curve*) at  $f = 17.2$  kHz. The zero point is offset in both for clarity. (b) Peak-to-peak cantilever response to oscillating heat input at a constant heating value of 1.89 mW as a function of heating frequency. A cantilever resonance peak appears at 17 kHz in air.

$d_{\text{H}_2\text{O}} = 53$  nm. According to Eq. (5), the ratio of cell temperatures should be proportional to the inverse ratio of the heat capacities. Assuming the tip deflection represents the cell temperature, the data give a ratio of  $d_{\text{air}}/d_{\text{H}_2\text{O}} = 1.26$ , while the ratio of heat capacities is  $(C_{p,\text{air}}/C_{p,\text{H}_2\text{O}})^{-1} = 2.23$ . These results indicate that the cantilever deflection reflects a cell temperature response that is accurately predicted by Eqs. (2) and (5). The differences observed between the measured and predicted thermal diffusivity and heat capacity ratios are likely the result of differences in heat losses that occur when the AFM cell contains air versus water.

These results indicate that the cantilever of an AFM can be used as a highly sensitive calorimeter. Previous reports suggest that as a bimetallic temperature sensor, an optimized AFM cantilever has a potential resolution of  $10^{-5}$  K and  $10^{-10}$  W.<sup>12</sup> However, current experimental constraints, including signal drift and the presence of nontrivial cantilever excitations from other noise sources, severely limit this projected resolution.

Noise sources in the AFM at ambient conditions, including unfiltered acoustic and mechanical vibrations as well as thermal noise, produce cantilever oscillations similar to that depicted in Fig. 4(a) (*upper curve*). Typical peak-to-peak oscillations approach 5 Å in air at room temperature. The can-

tilever functions as a mechanical filter, where these fluctuations are filtered at low frequencies and focused at the cantilever resonance frequency. For the 200- $\mu\text{m}$  cantilever, the resonance frequency is located near 17 kHz in air. The resonance frequency and fluctuation amplitude decrease when the cantilever is placed in liquid environments as a result of viscous damping. Cantilever fluctuations increase when an oscillating heat input is applied. In Fig. 4(a) (*lower curve*), a heat input of 0.47 mW ( $p-p$ ) near the resonance frequency ( $f_H = 17.2$  kHz) is seen to increase cantilever fluctuations from 5 Å to approximately twice that value. The magnitude of cantilever oscillation increases with increasing heat input. This increase follows a similar increase with heating power as was observed for cantilever deflections at constant heating rates. Thus, the magnitude of these fluctuations can be used to measure the system temperature response and thermal properties as was demonstrated with the dc response. In an ac measurement, however, signal drift can be eliminated from the cantilever response, which suggests a method for increasing the cantilever's response as a calorimeter.

The cantilever response to a fixed heating value is a function of the magnitude of heat input and to the frequency of the temperature fluctuations. In Fig. 4(b), the frequency-dependent response of a 200- $\mu\text{m}$  cantilever is plotted at a fixed input excitation of 1.89 mW. The theoretical response of the system temperature can be described, for example, by the solution to Fourier's equation for a semi-infinite solid with periodic heat flux. The steady-state portion of this solution takes the form

$$T = \frac{\tilde{F}\sqrt{\kappa/\omega}}{K} \exp\left(-x\sqrt{\frac{\omega}{2\kappa}}\right) \cos\left[\omega t - \frac{\pi}{4} - x\sqrt{\frac{\omega}{2\kappa}}\right] \quad (6)$$

where  $\tilde{F}$  is the magnitude of the heat oscillation and  $\omega$  ( $\omega = 2\pi f$ ) is the heating frequency. Thus, for oscillatory heating with a resistive heater, the wall temperature at  $x=0$  is governed by

$$T|_{\text{wall}} = \frac{\tilde{F}\sqrt{\kappa/\omega}}{K}. \quad (7)$$

Equation (7) suggests that the wall temperature should increase and be proportional to increasing heat input while the temperature should decrease with increasing heating frequency and be proportional to the inverse square root of the heating frequency. The cantilever oscillation for a fixed heat input as a function of heating frequency [Fig. 4(b)], measured with a lock-in amplifier, reflects an  $\omega^{-1/2}$  behavior at frequencies of 200 Hz and below. As the heating frequency is increased beyond this value, cantilever oscillations remain relatively constant until the resonance frequency of the cantilever is reached. At this heating frequency, tip oscillations increase as a resonance condition is obtained. Thus, cantilever oscillations are highly sensitive to a fluctuating heat input at low frequencies and near resonance.

#### IV. IMAGING RESULTS

In normal contact mode imaging, the static deflection of an AFM cantilever is used to detect and monitor surface topography. Typically, the tip is in direct contact with the

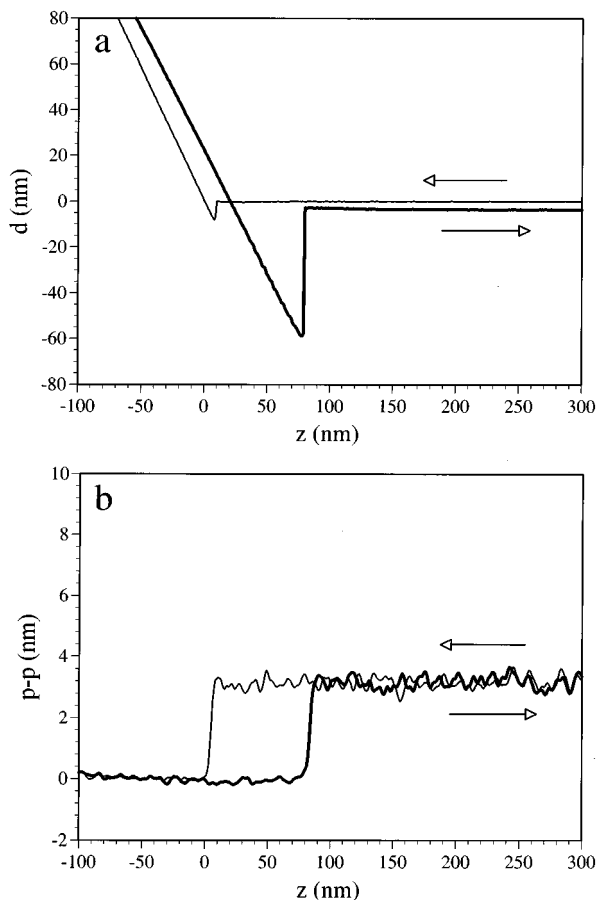


FIG. 5. Response of bimetallic cantilever probe in  $\text{H}_2\text{O}$  during approach (*thin line*) and retract (*thick line*) to a polished Ni-Cr substrate with 0.83 mW heating at 3.4 kHz. (a) Static cantilever deflection and (b) peak-to-peak amplitude tip oscillations.

sample during imaging in the contact mode. Thus, the tip lightly drags across the surface and topography is mapped as a feedback loop attempts to maintain a constant force, as determined by a constant tip deflection. This imaging mechanism is limited by the presence of lateral forces, which serve to damage soft samples and reduce image resolution by obscuring normal forces that are associated with purely topographical information. Also, the tip frequently sticks to features and skips across the surface; this degrades microscope resolution and creates characteristic streak features in an image. Although lateral forces are frequently used to image frictional properties on a surface, they are detrimental to pure topographical imaging.

In contact-mode AFM, a sample surface is detected by cantilever deflection. During approach to a sample in aqueous solution [Fig. 5(a), *thin line*], the cantilever will deflect toward the surface with a characteristic snap-in feature when van der Waals attractive forces exceed the spring constant of the cantilever. Once in contact with a surface, the deflection versus distance data become linear, reflecting a region of constant compliance. When the sample is then retracted from the sample [Fig. 5(a), *thick line*], the tip will snap away from the surface as van der Waals and tip-sample bonding forces are exceeded by the cantilever. The hysteresis between approach and retract curves represents the additional bonding

that occurs between tip and sample during contact. Under ambient conditions in air, the hysteresis is often considerably larger between approach and retract because a thin film of water present on the tip and sample produces capillary forces that must be overcome to break from this film. This liquid layer has proved somewhat troublesome for ac-mode imaging in air in these studies. When imaging in liquids, the hysteresis is reduced and a suitable set point is more easily maintained. The set point condition generally employed for contact imaging places the cantilever in the constant compliance region indicated by the linear regions in Fig. 5(a). The imaging force is defined as the force required to pull the tip away from the surface.

The primary advantage of ac-mode imaging is that lateral forces can be completely eliminated between the tip and sample, which greatly reduces the force imparted on the sample and generally improves image resolution. In ac-mode imaging, the cantilever is forced to oscillate by piezoelectric, acoustic, magnetic, or photothermal sources (*vide supra*). In the present configuration, resistive heating is used to oscillate the cantilever with a fluctuating heat input set to the resonant frequency of the cantilever. The peak-to-peak amplitude of oscillation can be set by the magnitude of the heating voltage. Generally, the free amplitude ranged from 1 to 15 nm. In Fig. 5(b), a heating input of 0.83 mW is applied to the resistive heater at a frequency of 3.4 kHz, which is near the resonance frequency of the 200- $\mu\text{m}$  cantilever in aqueous solutions. A similar response is obtained from the 100- $\mu\text{m}$  cantilever, with the resonance frequency between 8 and 12 kHz. When the tip is far from the substrate, the cantilever amplitude is near 3 nm. This oscillation is superimposed on the static cantilever deflection. Therefore, Figs. 5(a) and 5(b) were recorded simultaneously. When the tip approaches the sample [Fig. 5(b), *thin line*], the cantilever oscillation is relatively constant at its undamped amplitude. As the tip reaches the surface, the cantilever oscillation is damped. Damping occurs at a separation just slightly larger than the snap-in position observed in the static deflection [Fig. 5(a)]. The point at which damping occurs is dictated by the magnitude of cantilever oscillation, with larger oscillations being damped further from the surface. Once in contact with the surface, the amplitude drops to zero. If the cantilever is placed directly over the heater, the oscillation amplitude is frequently seen to increase on surface approach before damping occurs. This is likely the result of an increasing temperature as the tip approaches the heater. As the sample is retracted [Fig. 5(b), *thick line*], the cantilever remains effectively damped until the tip begins to snap away from the sample. At this point, the oscillations increase again until they reach the magnitude corresponding to an undamped cantilever.

The damping of cantilever oscillations at a fixed frequency can be used as a feedback signal in ac-mode imaging. Alternatively, as the tip and sample begin to interact, the resonance frequency will shift to lower values and the phase between oscillation and excitation will change. Thus, frequency and phase-shift detection systems can also be used in noncontact imaging.<sup>17,18</sup> The amplitude signal is used as a feedback signal for images presented here.

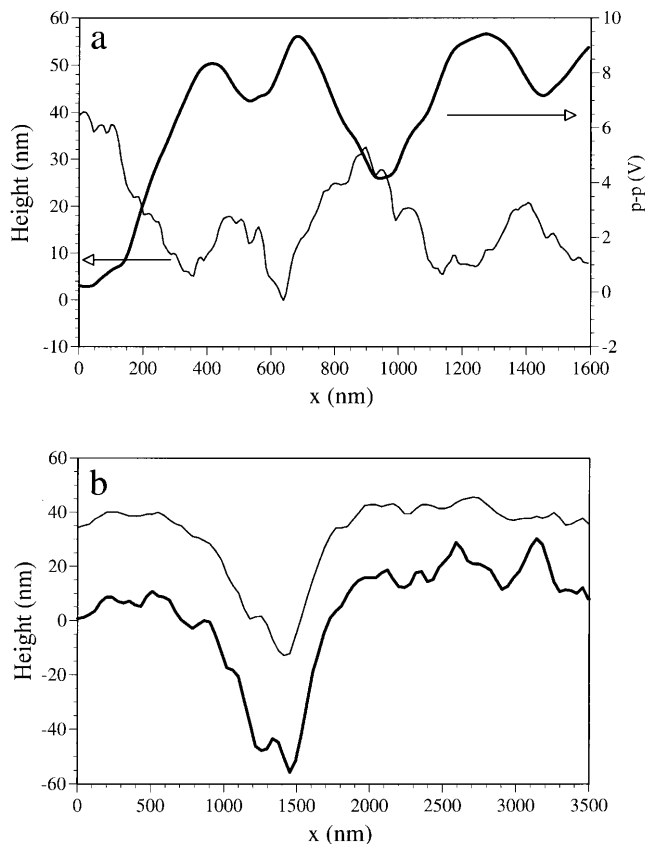


FIG. 6. Line scans of a polycrystalline nickel-chromium sample in  $H_2O$ . (a) Normal contact mode height image with feedback on at constant force conditions (*thin line*) and peak-to-peak tip oscillations with feedback off under constant height conditions (*thick line*). (b) Normal contact mode height image with feedback on at constant force conditions (*thin line*) and ac-mode height image with feedback on at constant damping conditions (*thick line*). ac-mode images were acquired with 0.83 mW heating at 3.4 kHz using the 200- $\mu\text{m}$  cantilever.

Figure 6(a) depicts a typical trace of sample height (*thin line*) and cantilever oscillation (*thick line*) as a polished polycrystalline Ni-Cr sample is rastered below a 200- $\mu\text{m}$  cantilever. The height data (*thin line*) was acquired during normal contact imaging and corresponds to the sample topography as the microscope feedback mechanism forces imaging to occur with a constant tip deflection. With the tip located near the surface and the feedback mechanism turned off, the thermally driven cantilever also responds to changes in surface topography. In this mode, the oscillations decrease from their free amplitude. The magnitude of this decrease depends upon the height of the surface features encountered. Thus, the contrast of this imaging mode is inverted from the topographic information, with large values for cantilever oscillation corresponding to sample recesses and a decrease in cantilever amplitude occurring when sample protrusions are encountered. When compared to the height data, the tip oscillations appear to have a lower resolution and are less sensitive to surface features. However, this is partially a result of the feedback mechanism being turned off, which leads to a variation in the tip-sample separation during scanning.

True topographic imaging can be achieved in this thermally driven cantilever system by replacing the existing deflection

signal in the feedback loop with one derived from the cantilever oscillation amplitude. This is achieved by inverting the amplitude signal and feeding it through the feedback channel of a homebuilt breakout box in the microscope [Fig. 1(a)]. A set point for imaging, which is defined as a fixed decrease in oscillation amplitude, is produced by offsetting the amplitude signal with a set-point voltage using a simple adder circuit. When imaging with the 100- and 200- $\mu\text{m}$  triangular cantilevers, the imaging speed was limited to near 1 Hz and below for a scan size of  $256 \times 256$  pixels. This resulted in image acquisition times of approximately 20 min per image. Faster scan speeds were limited by the oscillation period of the cantilever. However, cantilevers with higher resonant frequencies could easily be used to increase the scan speed, because the corresponding increase in spring constant with these cantilevers would have less of an impact on the applied force during ac-mode imaging. The higher spring constant of such a cantilever would also reduce the hysteresis between approach and retract curves, which is beneficial in non-contact imaging.

An example of a one-dimensional line scan in both normal contact and noncontact imaging modes in aqueous solution is shown in Fig. 6(b). The sample is a polished Ni-Cr wire. The substrate acts as both a surface for imaging and also as an excitation source for thermal heating. The line scan at normal contact mode conditions, where the cantilever deflection is used as a feedback signal, is shown [Fig. 6(b), *thin line*]. The tip is scanned over a crevice feature on the surface with a depth of about 50 nm. In ac mode, where the cantilever oscillation is used as a feedback signal, a comparable topographic scan is obtained [Fig. 6(b), *thick line*]. The essential features of the contact scan are retained when using the cantilever oscillation as a feedback parameter. However, the resolution appears to have improved. Features on the relatively flat regions away from the crevice are more clearly defined, as are structures located on the side walls of the crevice.

An example of a two-dimensional height image in both normal contact and non-contact imaging modes in aqueous solution is shown in Fig. 7. The sample is a piece of polished Delrin that was located approximately 1 mm away from a resistive heater. In general, the heater could be placed several millimeters away from the surface of interest and still provide sufficient energy to excite the cantilever at resonance. This is a result of the heater raising the temperature of the entire cell volume, not simply the region directly adjacent to the cantilever. The 100- $\mu\text{m}$  cantilever is used for imaging with a heating input of 1.89 mW at a frequency of 8.7 kHz. At this heating value, the free peak-to-peak cantilever oscillations are approximately 7 nm, as measured with the lock-in signal. During imaging, the bias is set so that cantilever oscillations are damped to approximately 30% of their free value. The contact image is shown in Fig. 7(a) and the ac-mode image is given in Fig. 7(b). The general features of the two images are the same. However, the ac-mode image is again of higher resolution, with finer surface structures being resolved. The contact image, in contrast, appears blurry. The blurriness of this image is concentrated along the raster direction, which is from left to right in the image, and results

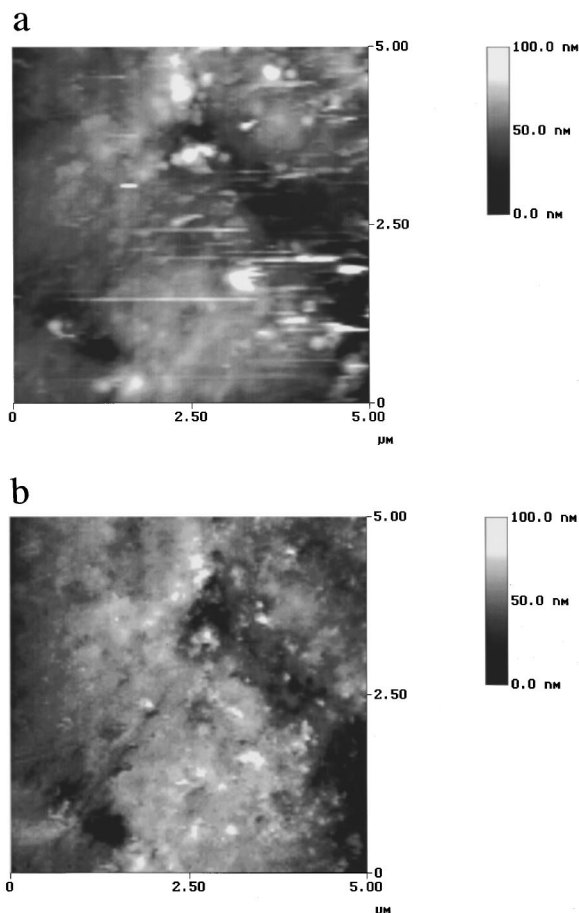


FIG. 7. Images of polished Delrin surface in  $H_2O$  under feedback conditions. (a) Normal contact mode AFM height image at a constant force condition and (b) ac-mode AFM height image at constant tip oscillation. The  $100\text{-}\mu\text{m}$  cantilever was used with  $1.89\text{ mW}$  heating at  $8.7\text{ kHz}$ .

from lateral forces as the tip drags along the sample from left to right during image acquisition. The ac-mode image is without the blur that corrupts the normal contact image. In this mode, rather than dragging the tip across the surface, the tip is oscillated vertically as it is rastered. In this particular image, the tip probably touches the surface during each oscillation and images in a tapping mode or intermittent-contact mode of operation.<sup>10,19</sup> The elimination of these lateral forces during imaging is the primary benefit of ac-mode imaging, because sample degradation is minimized and microscope resolution is enhanced. Images could be obtained over a range of set-point conditions with a variation in the amount of oscillation damping for imaging. The resolution decreased as the set point was lowered, corresponding to smaller damping of the free cantilever oscillation. Once the cantilever reached its free oscillation amplitude, the surface could generally not be sensed with the probe and the microscope disengaged.

## V. RECOMMENDATIONS

The results presented here demonstrate the first successful application of indirect, resistive heating to drive an ac-mode AFM. The novelty of this technique is that it is simple and may be used to convert a commercially available contact

AFM into an ac-mode microscope with the simple addition of a break-out box, resistive wire heater, wave form generator, either lock-in amplifier or rectifier circuit, and a simple adder circuit. When a rectifier circuit is used, all signal processing can be performed with homebuilt circuitry and only a wave form generator is required to excite the cantilever. The utility of this method is that it may be used in both gas and liquid environments, with the latter benefiting considerably from the elimination of lateral forces during imaging.

Improvements in this manner of ac-mode imaging may be achieved by using a cantilever with a larger spring constant and higher resonance frequency. A higher resonance frequency would allow data acquisition at faster rates and reduce the time required to obtain an image. A higher spring constant would decrease the hysteresis between approach and retract curves, which degraded the performance of the feedback loop for topographical imaging. This study has demonstrated the ability of an AFM cantilever to characterize thermal processes, and this area of research is being actively pursued by several groups.<sup>12-14,20</sup>

## ACKNOWLEDGMENTS

The authors gratefully acknowledge financial support from the Robert A. Welch Foundation and the National Science Foundation.

- <sup>1</sup>(a) G. Binnig, C. F. Quate, and Ch. Gerber, *Phys. Rev. Lett.* **56**, 930 (1986); (b) D. Sarid, *Scanning Force Microscopy*, edited by M. Lapp and H. Stork (Oxford University Press, Oxford, 1991); (c) D. Rugar and P. Hansma, *Phys. Today* **43**, 23 (1990).
- <sup>2</sup>(a) G. M. McClelland, R. Erlandsson, and S. Chiang, *Review of Progress in Quantitative Nondestructive Evaluation*, edited by D. O. Thompson and D. E. Chimenti (Plenum, New York, 1987), Vol 6B; (b) Y. Martin, C. C. Williams, and H. K. Wickramasinghe, *J. Appl. Phys.* **61**, 4723 (1987); (c) D. Rugar, H. J. Mamin, R. Erlandsson, J. E. Stern, and B. D. Terris, *Rev. Sci. Instrum.* **59**, 2337 (1988).
- <sup>3</sup>(a) T. Goddehenrich, H. Lemke, U. Hartmann, and C. Heiden, *J. Vac. Sci. Technol. A* **8**, 383 (1990); (b) G. Neubauer, S. R. Cohen, G. M. McClelland, D. Horne, and C. M. Mate, *Rev. Sci. Instrum.* **61**, 2296 (1990); (c) S. A. Joyce and J. E. Houston, *Rev. Sci. Instrum.* **62**, 710 (1991).
- <sup>4</sup>(a) A. J. den Boef, *Rev. Sci. Instrum.* **62**, 88 (1991); (b) S. Grafstrom, J. Ackermann, T. Hagen, R. Neumann, and O. Probst, *J. Vac. Sci. Technol. B* **12**, 1559 (1994).
- <sup>5</sup>W. A. Ducker, R. F. Cook, and D. R. Clarke, *J. Appl. Phys.* **67**, 4045 (1990).
- <sup>6</sup>J. O'Shea, M. E. Welland, and J. B. Pethica, *Chem. Phys. Lett.* **223**, 336 (1994).
- <sup>7</sup>(a) N. Umeda, S. Ishizaki, and H. Uwai, *J. Vac. Sci. Technol. B* **9**, 1318 (1991); (b) O. Marti, A. Ruf, M. Hipp, H. Bielefeldt, J. Colchero, and J. Mylnek, *Ultramicroscopy* **42-44**, 345 (1992); (c) J. Mertz, O. Marti, and J. Mlynek, *Appl. Phys. Lett.* **62**, 2344 (1993).
- <sup>8</sup>A. Vinckier, F. Hennau, K. Kjoller, and L. Hellemans, *Rev. Sci. Instrum.* **67**, 387 (1996).
- <sup>9</sup>M. A. Lantz, S. J. O'Shea, and M. E. Welland, *Appl. Phys. Lett.* **65**, 409 (1994).
- <sup>10</sup>P. K. Hansma, J. P. Cleveland, M. Radmacher, D. A. Walters, P. E. Hillner, M. Bezaniilla, M. Fritz, D. Vie, H. G. Hansma, C. B. Prater, J. Massie, L. Fukunaga, J. Gurley, and V. Elings, *Appl. Phys. Lett.* **64**, 1738 (1994).
- <sup>11</sup>R. J. Roark and W. C. Young, *Formulas for Stress and Strain*, 5th ed. (McGraw-Hill, New York, 1975).
- <sup>12</sup>J. R. Barnes, R. J. Stephenson, C. N. Woodburn, S. J. O'Shea, M. E. Welland, T. Rayment, J. K. Gimzewski, and Ch. Gerber, *Rev. Sci. Instrum.* **65**, 3793 (1994).
- <sup>13</sup>J. K. Gimzewski, Ch. Gerber, E. Meyer, and R. R. Schlittler, *Chem. Phys. Lett.* **217**, 589 (1994).
- <sup>14</sup>(a) O. Nakabeppu, M. Chandrachood, Y. Wu, J. Lai, and A. Majumdar,

- Appl. Phys. Lett. **66**, 694 (1995); (b) A. Majumdar, J. Lai, M. Chandrachud, O. Nakabeppu, Y. Wu, and Z. Shi, Rev. Sci. Instrum. **66**, 3584 (1995).
- <sup>15</sup>J. E. Sader, Rev. Sci. Instrum. **66**, 4583 (1995).
- <sup>16</sup>H. S. Carslaw and J. G. Jaeger, *Conduction of Heat in Solids*, 2nd ed. (Oxford University Press, New York, 1959).
- <sup>17</sup>Y. Martin, C. C. Williams, and H. K. Wickramasinghe, J. Appl. Phys. **61**, 4723 (1987).
- <sup>18</sup>A. Kikukawa, S. Hosaka, Y. Honda, and R. Imura, Rev. Sci. Instrum. **66**, 101 (1995).
- <sup>19</sup>(a) Q. Zhong, D. Inness, K. Kjoller, and V. B. Elings, Surf. Sci. Lett. **290**, L688 (1993); (b) C. A. J. Putman, K. O. van der Werf, B. G. de Groot, N. F. van Hulst, and J. Greve, Appl. Phys. Lett. **64**, 2454 (1994).
- <sup>20</sup>(a) T. Thundat, R. J. Warmack, G. Y. Chen, and D. P. Allison, Appl. Phys. Lett. **64**, 2894 (1994); (b) T. Thundat, G. Y. Chen, R. J. Warmack, D. P. Allison, and E. A. Wachter, Anal. Chem. **67**, 519 (1995).